Thin Solid Films 517 (2009) 1731–1735

Contents lists available at ScienceDirect

Thin Solid Films

journal homepage: www.elsevier.com/locate/tsf

Al_2O_3/SiO_2 and HfO_2/SiO_2 dichroic mirrors for UV solid-state lasers

Maria Luisa Grilli [a], Francesca Menchini [a,*], Angela Piegari [a], Daniele Alderighi [b], Guido Toci [b], Matteo Vannini [b]

[a] Optical Coatings Group, Physics Technologies and Materials Division, ENEA, Via Anguillarese 301, 00123 Rome, Italy
[b] IFAC-CNR, Via Madonna del Piano, 50019 Sesto Fiorentino (FI), Italy

ARTICLE INFO

Article history:
Received 4 December 2007
Received in revised form 30 July 2008
Accepted 14 September 2008
Available online 22 September 2008

Keywords:
Optical coatings
Oxides
UV laser

ABSTRACT

HfO_2/SiO_2 and Al_2O_3/SiO_2 multilayers to be employed as high reflectance end mirrors in Cerium-doped fluoride solid-state lasers were produced by radio frequency sputtering. The components were designed to have high transmittance at the pumping wavelength and high reflectance in a wavelength band corresponding to the active medium emission. A photoacoustic beam deflection technique and inspection of the irradiated area under a microscope were used to measure the laser induced damage threshold of the mirrors at the pumping wavelength. These coatings were tested in a laser cavity.

1. Introduction

Over the past few years great interest has been directed to the development of solid-state lasers providing direct emission in the near UV. Several Ce-doped fluoride solid-state lasers were proposed [1,2], which produce tunable output in the range 280–330 nm. Dichroic mirrors to be used as end mirrors (EM) in a laser cavity with collinear pumping geometry have strict requirements: they should provide a high transmittance at the pumping wavelength together with a high reflectance at the output laser wavelength, these two wavelengths being very close to each other. Moreover, high laser induced damage thresholds (LIDT) are required both at the pumping and at the laser wavelengths.

It is difficult to find commercial products which satisfy all the requirements of these lasers because of the specificity of each laser material and different pumping geometries. Custom-made solutions are necessary for different applications.

For the fabrication of high quality optical interference components for UV-applications, materials with low absorption, low scattering levels and high laser damage thresholds are necessary. Hafnium oxide (HfO_2) has been widely chosen as the high index material for the manufacture of interference coatings in the UV spectral region, in combination with silicon dioxide (SiO_2) as the low-index material [3–6]. Aluminum oxide (Al_2O_3) is sometimes preferred to HfO_2 due to its higher transparency at wavelengths shorter than 250 nm, even though its refractive index is closer to that of SiO_2 and a larger number of layers is needed. Mirrors with high LIDT can be fabricated using Al_2O_3 [7,8].

In this study, dichroic mirrors with SiO_2, Al_2O_3 and HfO_2 were fabricated by radio frequency (r.f.) sputtering. The design requirement is a high reflectance over the range 280–315 nm, corresponding to the active-crystal emission band. A high transmittance is also required at 263 nm (266 nm), the pumping wavelength provided by the fourth harmonic of Nd:YLF (Nd:YAG) source. Laser induced damage thresholds at 263 nm were measured by the photoacoustic (PA) beam deflection technique [9–11]. These coatings were then tested in a laser cavity with a collinear geometry.

2. Experimental details

Single SiO_2, Al_2O_3 and HfO_2 layers were deposited on fused silica substrates (Quartz Heraeus) by r.f. sputtering. The sputtering targets were 16.5 cm diameter sintered metal oxides of 99.99% nominal purity. A base pressure below 2×10^{-4} Pa was ensured in the deposition chamber by a turbomolecular pump. Both HfO_2 and SiO_2 films were deposited at a r.f. power of 400 W in an Ar + O_2 atmosphere (oxygen partial pressure about 67%) at a working pressure of 1.2 Pa. Al_2O_3 films were grown in pure Ar atmosphere at 1.0 Pa and r.f. power of 350 W. Deposition rates were 1.7, 2.3 and 2.0 nm/min for HfO_2, SiO_2 and Al_2O_3 films, respectively. Sample temperature during the deposition was not controlled, but raised to 190 °C during the single layers deposition and to 250 °C during the multilayers deposition, due to plasma heating. Film thickness was monitored by a quartz oscillator.

Transmittance and reflectance were measured in the UV–VIS optical range (200–800 nm) using a Perkin-Elmer Lambda 900 spectrophotometer, both on single layer coatings and on the dichroic mirrors. Total scattering was measured on the same samples using an attachment to the commercial spectrophotometer [12]. X-ray diffraction analysis was performed on the single layers using a Philips X-Per Pro 500 Diffractometer with Cu K_α radiation (λ=0.154 nm) at a fixed grazing angle incidence of 1°. The microstructure of the films was

* Corresponding author. Tel.: +39 06 30483901; fax: +39 06 30486364.
E-mail address: francesca.menchini@casaccia.enea.it (F. Menchini).

0040-6090/$ – see front matter © 2008 Elsevier B.V. All rights reserved.
doi:10.1016/j.tsf.2008.09.047

studied by a field emission scanning electron microscope (Leo Supra 35). SEM images were obtained at an accelerating voltage EHT of 5 kV.

The LIDT of the dichroic mirrors was measured using a dedicated set-up (see Fig. 1), based on the principle of photoacoustic beam deflection, which will be described in Section 3.3. The 263 nm heating radiation was generated by a quadrupled Nd:YLF laser with 6 ns (Full Width Half Maximum) pulse duration. This laser can be operated using external triggering, which permits both single and multiple (10 Hz) pulse excitation. A small fraction of the Nd:YLF beam was sent to a calibrated energy monitor for the single-pulse energy measurement and to a CCD camera for the single-pulse spatial profile measurement. The remaining high-intensity beam illuminated the sample. The heating beam and the low-intensity beam sent to the CCD were both focused in the vertical direction by means of two identical cylindrical lenses. With this set-up, for each pulse impinging on the sample it is possible to measure simultaneously both the single-pulse energy and the spatial intensity distribution on the lens focal plane, so that the measurements are not affected by the laser pulse-to-pulse fluctuation, as it would happen by acquiring the PA signal, the pulse energy and the beam profile on different pulses.

A He–Ne laser probe beam was focused by a 40 cm focal spherical lens in a spot having a diameter of 370 μm (at $1/e^2$ of the peak); the beam waist overlapped the heating spot approximately 1 mm away from the sample surface. By means of a cylindrical lens, the heating beam was focused in an elliptical spot (about 600 μm long and 60 μm wide at $1/e^2$ of the peak fluence), with the longer axis parallel to the probe beam. The probe beam was collinearly oriented with the longer axis of the elliptical heating spot. We adopted this geometry, instead of the usual spherical focusing on a circular spot, in order to compensate for the relatively low energy of the excitation pulse. Indeed, the probe beam deflection angle ϕ is given by [13]

$$\phi = \frac{1}{n_{\text{air}}} \int_{\text{path}} \nabla_{\perp} n_{\text{air}} \mathrm{d}S, \tag{1}$$

where n_{air} is the refractive index of the surrounding air, the integral is carried out along the probe beam path, and $\nabla_{\perp}$ is the gradient in the direction perpendicular to the beam path. For given interaction path length and heating pulse energy, the cylindrical focusing allows to obtain a higher fluence than that obtained with a spherical focusing (i.e. on a circular spot), because the size of the beam in the direction perpendicular to the probe beam path can be reduced.

The probe beam then illuminated a vertical single knife-edge, which blocked half of the beam profile. The transmitted beam was finally focused on a photodiode connected to an oscilloscope for the photoacoustic signal detection.

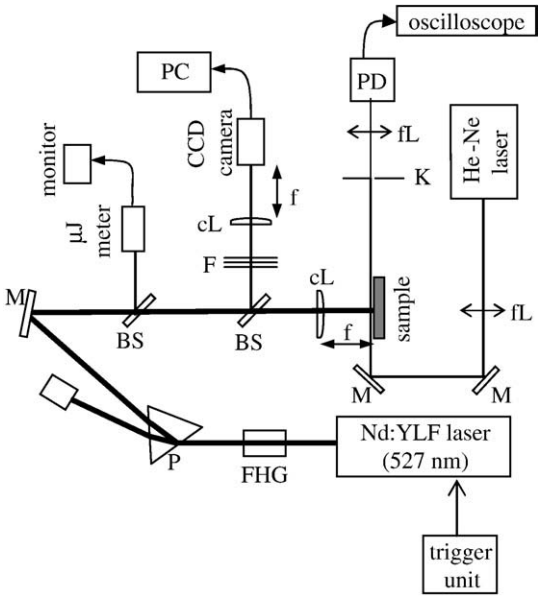

Fig. 1. Experimental set-up for the determination of laser induced damage thresholds: P, quartz prism; M, aluminized flat mirror; BS, tilted quartz window; cL, cylindrical lens; F, neutral density filters; K, one edge knife; fL, focusing lens; PD, photodiode.

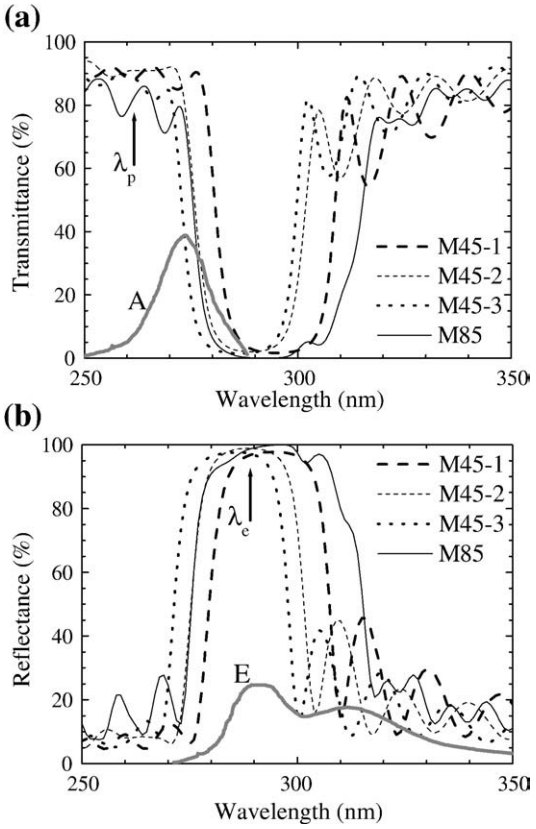

Fig. 2. Transmittance (a) and reflectance (b) spectra of Al_2O_3/SiO_2 multilayers. The absorption (A) and emission (E) profiles of the Ce:LiCAF crystal are also reported in arbitrary units.

3. Results and discussion

3.1. SiO_2, Al_2O_3 and HfO_2 single layers

The optical constants and the thickness of the films were calculated using commercial software to fit the experimental spectrophotometric data. Silica films show practically no absorption. Alumina films show low k values, in agreement with data reported in the literature: at 250 nm k is lower than 1.1×10^{-3}, which is comparable to results obtained on PIAD [14] or reactive sputtered films [15]. For hafnia films, k is lower than 6×10^{-3} at 250 nm, but increases dramatically below 230 nm. Such k values are higher than data reported for reactive evaporated coatings [6,14], but comparable to data reported for PIAD films [14].

From X-ray diffraction measurements, an amorphous structure was found both for alumina and silica films, while a monoclinic structure (JCPDS 78-00500) was found for hafnia coatings. The assignment of the diffraction peaks has been done using the PCPDFWIN database. The morphology of hafnia coatings was characterised by a homogeneous distribution of nano-sized grains.

3.2. Multilayers

Based on the above-described materials, several multilayer coatings were deposited employing HfO_2 and SiO_2 (M20-n) and Al_2O_3 and SiO_2 (M45-n and M85).

The starting coating design for all samples is a stack of alternating high- (H) and low- (L) index materials with the structure described in the following.

In samples M45-*n* the first and last low-index layers have eighth-wave thickness while the other layers have quarter-wave thickness (QWOT). M45-*n* mirrors differ in the reference wavelength or in the film growth rate. Sample M85 is made by two quarter-wave overlapping multilayers with shifted reference wavelengths, deposited on the same substrate surface; in this way a wider reflectance band is achieved, even though the number of layers is increased up to 85. In mirrors M20-*n*, the increase in UV transmittance is obtained by modifying the optical thicknesses of three layers with respect to the QWOT. The final designs of the above-mentioned mirrors are the following:

M45–*n* sub/0.5L/$(HL)^{21}$/H/0.5L/air

M85 sub/0.48L/$(0.97H/0.97L)^{20}$/0.97H/0.98L/0.98H/L/$(1.01H/1.01L)^{2}$/ /1.01H/$(1.02L/1.02H)^{10}$/$(1.03L/1.03H)^{7}$/0.52L/air

M20–*n* sub/1.12H/1.22L/$(H/L)^{8}$/H/0.48/air

where the reference wavelength is in the range 285–315 nm.

The transmittance and reflectance spectra of the mirrors are shown in Figs. 2 and 3, and the main properties are summarized in Table 1. In sample M85, the bandwidth has increased up to 39 nm, which permits a greater range of tunability of the output laser radiation. For the M20-*n* mirrors, a larger bandwidth and a comparable reflectance are obtained with a smaller number of layers because of the higher refractive index of HfO_2 with respect to that of Al_2O_3.

Table 1
Multilayer coating characteristics

Sample	Materials	Number of layers	High reflectance band center (nm)	Band width FWHM (nm)	Max reflectance (%)	Transmittance at 263 nm (%)
M45-1	Al_2O_3/SiO_2	45	295	28	98±1	90.0±0.5
M45-2	Al_2O_3/SiO_2	45	290	26	97±1	91.0±0.5
M45-3	Al_2O_3/SiO_2	45	286	26	98±1	87.0±0.5
M85	Al_2O_3/SiO_2	85	296	39	99±1	85.0±0.5
M20-4	HfO_2/SiO_2	20	311	65	97±1	73.2±0.5
M20-5	HfO_2/SiO_2	20	313	64	97±1	74.1±0.5
M20-6	HfO_2/SiO_2	20	311	67	97±1	74.9±0.5

For all M45-*n* mirrors, the optical losses (scattering + absorption) at the reference wavelength are lower than 1.5%; losses at the pumping laser wavelength vary from one coating to another in the range 1–3%. For M85 mirror, the losses are less than 1% and 3% at the reference wavelength and the pumping wavelength, respectively. For M20-*n* mirrors, the total losses at the reference wavelength vary in the range 2–3%, but they increase significantly (up to 20%) at the pumping wavelength. It was found that scattering gives a high contribution to such losses, probably due to the crystalline structure of the HfO_2 layers.

3.3. Laser-induced damage threshold measurements

It is well known that when a high power laser pulse is focused on a sample, part of its energy can be absorbed by the sample and converted into heat via non-radiative processes. The medium around the irradiated area of the sample thus expands, inducing a pressure (acoustic) wave. The pressure and temperature variations produce a

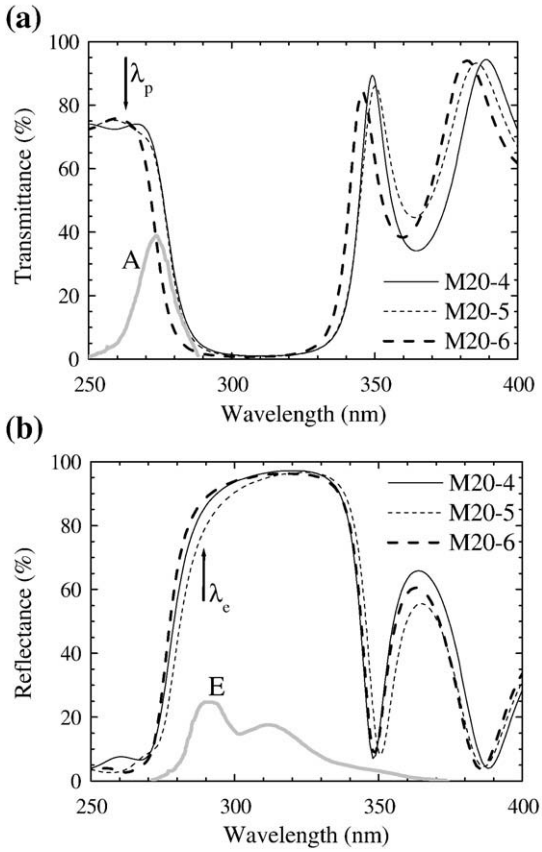

Fig. 3. Transmittance (a) and reflectance (b) spectra of the HfO_2/SiO_2 multilayers. The absorption (A) and emission (E) profiles of the Ce:LiCAF crystal are also reported in arbitrary units.

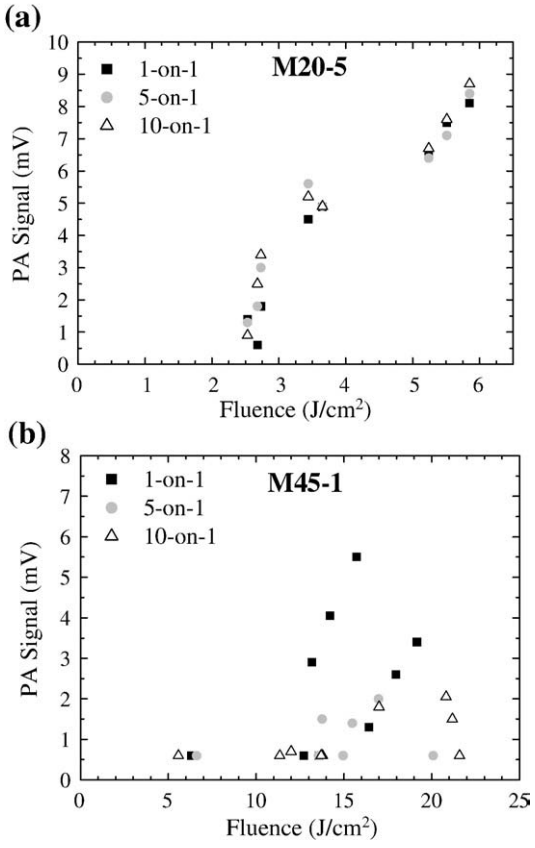

Fig. 4. Photoacoustic signal on samples M20-5 (a) and M45-1 (b).

Table 2
1-on-1 LIDT values

Sample	LIDT (J/cm^2)	Visible damage
M45-1	10±1*	No
M45-2	7±1*	No
M45-3	7±1*	No
M85	7±1*	No
M20-4	2.0±0.2	Yes
M20-5	1.8±0.2	Yes
M20-6	1.6±0.2	Yes

*These values have to be considered as a prudential lower limit.

refractive index gradient in the air near the sample and, as a consequence, a probe beam passing parallel to the surface is deflected. A description of the principle of the photoacoustic and photothermal beam deflection technique is given in the literature [9–11].

In this work, a set of PA deflection measurements from different sites on the fabricated samples was recorded after 1, 5 and 10 laser pulses. The laser fluence was increased for each new test site, obtaining three series of data. Fig. 4 shows the results of the measurements on some of the investigated mirrors.

For all the HfO_2-based samples, a typical threshold-like trend was found (Fig. 4a), common to each series of data. For the 1-on-1 mode, LIDT values were found in the range of 1.6–2 J/cm^2 (Table 2), comparable with data reported in the literature for similar multilayers. The damage was visible to the naked eye and was confirmed by inspection under the optical microscope.

No evidence of irreversible damage was found for the Al_2O_3-based samples, neither in the photoacoustic data nor after inspection by eye or under the microscope for the available fluences of our set-up. For these samples (see Fig. 4b), we have found that the PA signal develops for incident fluences above a threshold spanning between 7 and 10 J/cm^2 (depending on the mirror design), but we could not find a clear trend in the behavior of the PA signal for increasing fluences above this threshold or for increasing number of shots on the same site. Furthermore, even in presence of a PA signal the irradiated sites did not show visual evidence of damage when inspected under the microscope. We did not check whether the PA data are reversible. Nonetheless, considering the onset of the PA signal as an indicator of the starting of a damage process, a prudential lower limit for the damage threshold of these mirrors can be set between 7 and 10 J/cm^2 (Table 2).

3.4. Laser tests

The results discussed in Sections 3.2 and 3.3 show that Al_2O_3/SiO_2 stacks are best suited for the laser applications described in the introduction. On the basis of M45-*n* design, the M45-5 coating was grown on the concave side of a 6 mm thick quartz (250 mm radius of curvature) to be used as the end mirror in the laser cavity shown in Fig. 5. Without spectral selection, laser oscillation in this cavity is obtained at 289 nm, the peak emission wavelength of the active medium. In order to verify the long term stability of these mirrors, the laser was driven at the repetition rate of 1 kHz. For comparison in the same cavity, a commercial mirror M1 which has higher reflectance (98.9%) at 289 nm but lower transmittance (66%) at 263 nm with respect to M45-5 (R_{289}=95% and T_{263}=89%) was used.

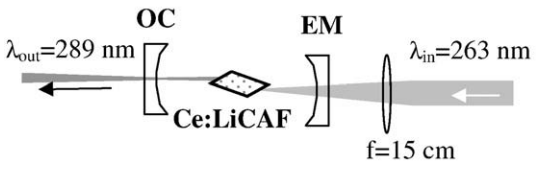

Fig. 5. Collinear cavity used for the laser tests.

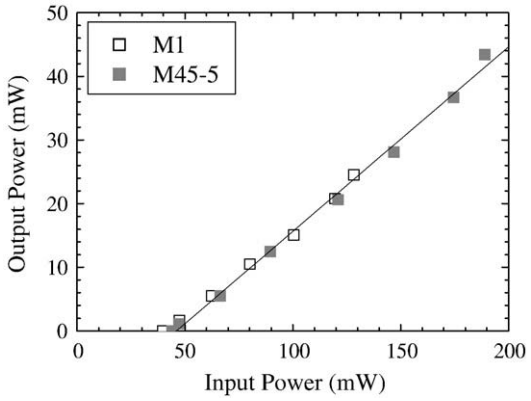

Fig. 6. Laser characteristics (output against input power) for a commercial mirror M1 and for mirror M45-5.

Fig. 6 shows the laser characteristics at 289 nm obtained using each type of mirror. The thresholds and slopes of the two curves, which depend on the crystal's characteristics and on the cavity losses, are comparable. With the same power delivered from the Nd:YLF pump laser, a higher output power can be extracted from the cavity in which the M45-5 mirror is employed. These results show that our sample allows a better exploitation of the pump source and higher pump levels on the crystal, with the same cavity losses and stability characteristics provided by the commercial mirror. Moreover, the transmittance of the mirrors could be further increased by 4% by depositing an AR coating at 263 nm on the back side, giving the advantage of high pump wavelength transmittance.

4. Conclusions

HfO_2/SiO_2 and Al_2O_3/SiO_2 multilayer systems to be used as high reflectance end mirrors in Ce-doped fluorides solid-state laser cavities were fabricated. Reflectance values in the range 97–99% were achieved together with high transmittance at the pumping wavelength. Comparable maximum reflectance and wider tunability were obtained for HfO_2/SiO_2 multilayer coatings, even though lower transmittance and lower laser induced damage thresholds were measured at the pumping wavelength with respect to Al_2O_3-based mirrors. High transmittance values at the pumping wavelength up to 91% and high laser induced damage thresholds up to 10 J/cm^2 were measured for Al_2O_3/SiO_2 coatings.

When used in a laser cavity with collinear pumping, our mirror achieved the same slope efficiency, threshold power, cavity losses and structural stability as those obtained with a commercial mirror, but with a better exploitation of the laser pump power.

Acknowledgements

This work was funded by the Minister of University and Scientific Research (MIUR) in the frame of the project “Impianti innovativi multiscopo per la produzione di radiazione X e ultravioletta, coerente ed incoerente ad alta intensità per applicazioni avanzate nel campo delle strutture biologiche, molecolari e dei materiali”.

References

[1] D.W. Coutts, A.J.S. Mc Gonigle, IEEE J. Quantum Electron. 40 (2004) 1430 (and references therein).
[2] D. Alderighi, G. Toci, M. Vannini, M. Mazzoni, M. Tonelli, D. Parisi, H. Sato, M. Niklc, in: I.A. Shcherbakov, A. Giardini, V.I. Konov, V.I. Pustovoy (Eds.), Advanced Laser Technologies 2004, Rome and Frascati, Italy, September 10, 2004, Proc. SPIE 5850, 2004, p. 362.
[3] F. Rainer, H.W. Lowdermilk, D. Milam, C.K. Carniglia, T. Tuttle Hart, T.L. Lichtenstein, Appl. Opt. 24 (1985) 496.
[4] R. Thielsh, T. Feigl, N. Kaiser, S. Martin, S. Scaglione, F. Sarto, M. Alvisi, A. Rizzo, in: G.J. Exarhos, A.H. Guenther, M.R. Kozlowski, K.L. Lewis, M.J. Soileau (Eds.), Laser-

Induced Damage in Optical Materials: Boulder, CO, USA, October 4, 1999, Proc. SPIE 3902, 1999, p. 182.
[5] P. Baumeister, O. Arnon, Appl. Opt. 16 (1977) 439.
[6] P. Torchio, A. Gatto, M. Alvisi, G. Albrand, N. Kaiser, C. Amra, Appl. Opt. 41 (2002) 3256.
[7] N. Kaiser, H. Uhlig, U.B. Schallenberg, B. Anton, U. Kaiser, K. Mann, E. Eva, Thin Solid Films 260 (1995) 86.
[8] M. Zhan, Y. Zhao, G. Tian, H. He, J. Shao, Z. Fan, Appl. Phys. B 80 (2005) 1007.
[9] A. Rosencwaig, J.B. Willis, Appl. Phys. Lett. 36 (1980) 667.
[10] S. Petzoldt, A.P. Elg, M. Reichling, J. Reif, E. Matthias, Appl. Phys. Lett. 53 (1988) 2005.
[11] D. Riso, M.R. Perrone, A. Piegari, M.L. Protopapa, S. Scaglione, J. Vac. Sci. Technol. A 18 (2000) 477.
[12] M.L. Grilli, A. Krasilnikova, F. Menchini, A. Piegari, in: A. Duparré, R. Geyl, L. Wang (Eds.), Proc. SPIE 5965, Jena, Germany, September 13, 2005, p. 566 (2005).
[13] W.B. Jackson, N.M. Amer, A.C. Boccara, D. Fournier, Appl. Opt. 20 (1981) 1333.
[14] R. Thielsh, A. Gatto, J. Heber, N. Kaiser, Thin Solid Films 410 (2002) 86.
[15] S.M. Edlou, A. Smajkiewicz, G.A. Al-Jumainly, Appl. Opt. 32 (1993) 5601.